THE JOURNAL OF PHYSICAL CHEMISTRY C

Article

pubs.acs.org/JPCC

Machine Learning Assisted Predictions of Intrinsic Dielectric Breakdown Strength of ABX_3 Perovskites

Chiho Kim,[†] Ghanshyam Pilania,[‡] and Rampi Ramprasad*[,†]

[†]Department of Materials Science & Engineering, and Institute of Materials Science, University of Connecticut, 97 North Eagleville Road, Storrs, Connecticut 06269-3136, United States

[‡]Materials Science and Technology Division, Los Alamos National Laboratory, Los Alamos, New Mexico 87545, United States

Supporting Information

ABSTRACT: New and improved dielectric materials with high dielectric breakdown strength are required for both high energy density electric energy storage applications and continued miniaturization of electronic devices. Despite much practical significance, accurate *ab initio* predictions of dielectric breakdown strength for complex materials are beyond the current state-of-the art. Here we take an alternative data-enabled route to address this design problem. Our informatics-based approach employs a transferable machine learning model, trained and validated on a limited amount of accurate data generated through laborious first-principles computations, to predict intrinsic dielectric breakdown strength of several hundreds of chemical compositions in a highly efficient manner. While the adopted approach is quite general, here we take up a specific example of perovskite materials to demonstrate the efficacy of our method. Starting from several thousands of compounds, we systematically downselect 209 insultors which are dynamically stable in a perovskite crystal structure. After making predictions on these compounds using our machine learning model, the intrinsic dielectric breakdown strength was further cross-validated using first-principles computations. Our analysis reveals that boron-containing compounds are of particular interest, some of which exhibit remarkable intrinsic breakdown strength of almost 2 GV/m.

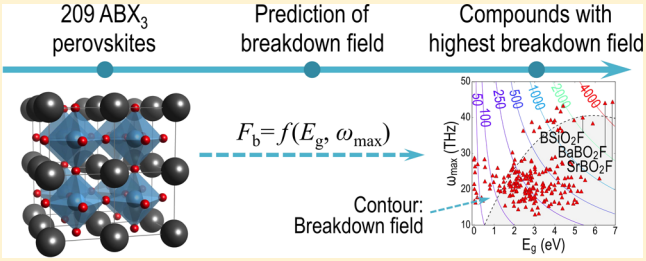

INTRODUCTION

Some of the critical challenges of our times are concerned with designing novel and improved materials to meet the rapidly rising demands for electric power and to sustain the ongoing electrical/electronic device miniaturization trends. Increasing the capacity of the electric power infrastructure to meet this growing demand requires operation at higher electric fields than is currently possible.[1] Likewise, miniaturization of electrical and electronic devices (while preserving or increasing their performance or functionality) requires ever thinner insulating dielectric layers that will soon experience enormous electric fields.[2] The present choices of materials, dimensions, and fields are limited by the dielectric breakdown of the insulation in operating conditions. Thus, novel materials with improved electric field tolerance are required to push further technological advancements in the fields of electrical insulation[3,4] and photovoltaic applications.[5−10]

The dielectric breakdown process is a highly complex phenomenon that represents an example of a "weakest link" problem. Breakdown strength of a material derives its contributions from both *intrinsic*[11−14] (i.e., dictated purely by chemical constituents, details of the crystal structure, and nature of the chemical bonding) and *extrinsic*[15−21] (i.e., defects, impurities, morphology, interfaces, field-induced aging, and degradation) factors. While a precise quantification of the role played by various extrinsic factors in determination of the dielectric breakdown is still beyond the current state-of-the-art, recently implemented quantum mechanical methods for the calculation of electron−phonon scattering rates have allowed for a completely first-principles quantitative determination of the intrinsic breakdown field of any insulator.[22] Within this parameter free computational framework based on classical theory formulated by von Hippel[11] and Fröhlich,[12,23,24] the breakdown criterion can be formulated as the lowest field at which the average electron energy gain from the field is greater than the average energy loss to phonons for all electron energies less than that which produces charge carrier multiplication through impact ionization. Within this framework, the computed dielectric breakdown strength of several insulators has been shown to agree remarkably well with the experimental results reported in the literature.[22,25,26]

In principle, one can use the aforementioned first-principles framework to compute intrinsic breakdown strength of plethora of materials in order to identify promising candidate materials. However, in practice, the computational cost associated with the formalism renders it highly inefficient for such high throughput explorations in vast chemical spaces. To circumvent this problem, we resort to a data-enabled informatics approach,

Received: May 19, 2016
Revised: June 17, 2016
Published: June 22, 2016

© 2016 American Chemical Society

DOI: 10.1021/acs.jpcc.6b05068
J. Phys. Chem. C 2016, 120, 14575−14580

where a machine learning method is first trained using a limited amount of first-principles data on selected compounds to establish a validated mapping between some easily accessible key attributes (also referred to as features or descriptors) of materials and the property of interest—the intrinsic breakdown strength. In fact, such a mapping was successfully demonstrated in our recent work on 82 octet AB-type crystalline solids, where three independent machine learning models were employed to give accurate predictions on the intrinsic breakdown strength over 3 orders of magnitude.[26] More interestingly, all the machine learning models converged to a single most important feature pair consisting of the band gap and the phonon cutoff frequency (i.e., the maximum phonon frequency at the Γ-point). The significance of this finding lies in the fact that the two identified features can be computed at a much lower computational cost for any given material crystal structure and composition, allowing for an efficient pathway toward predicting the intrinsic breakdown strength without explicitly pursuing the expensive first-principles framework. In our previous work we also demonstrated the generalizability of the adopted machine learning framework by predicting the breakdown strength of materials with different crystal structures and chemical compositions than those in the original training set.

In this contribution, we further build on our past work by employing the developed machine learning framework by screening a large number of perovskite materials in order to identify candidates with high intrinsic dielectric breakdown. Given the fact that about 90% of the periodic table can be synthesized in a stable perovskite crystal structure, and given that a number of perovskites have already been suggested as potential next-generation dielectric materials,[3,5,7,8,10] these materials naturally lend themselves as ideal candidates for such a high throughput exploration. We start with a target chemical space containing ∼19 000 ABX_3 type perovskites which were reported previously,[27] where A and B represent metal cations and the motif X_3 can take one of the seven possibilities, viz., N_3, O_2F, O_2N, O_2S, O_3, OFN, and ON_2 (cf. Figure 1). Out of these 19 000 compounds, only 735 materials were found insulating (based on the CMR reported GLLB-SC band gaps). For each of these materials a structure reoptimization was performed using density functional theory (DFT) computations and their dynamical stability was assessed by computing phonon dispersions. Subsequently, 209 dynamically stable ABX_3 compounds were identified, for which accurate band gaps were predicted using the hybrid Heyd–Scuseria–Ernzerhof (HSE06) exchange-correlation functional.[28] As depicted in Figure 1, these dynamically stable insulating perovskites reveal a rich spectrum of theoretical band gaps (from slightly larger than 0 eV to less than 7 eV) and maximum phonon frequency (up to 44 THz), the two descriptors relevant for the prediction of the intrinsic breakdown strength. For completness, although they are not relevant to the present study, histograms of the atomization energies, lattice constants, and material densities are also presented in Figure 1 for these 209 compounds.

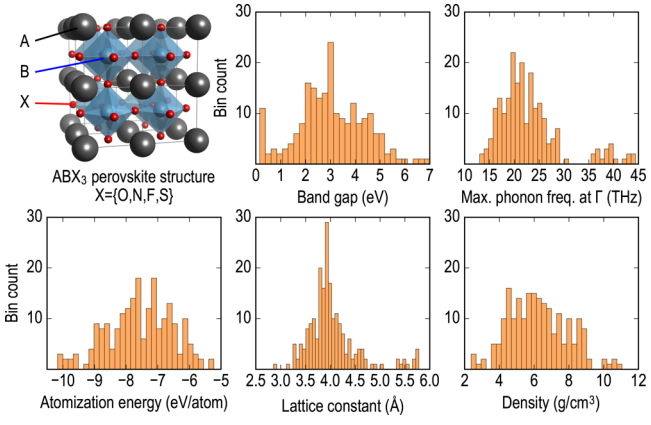

Figure 1. Perovskite crystal structure with rocksalt ordering of both A- and B-site cations. Histogram of band gap, maximum phonon frequency at Γ point, atomization energy, lattice constant, and density of perovskites used in the prediction of intrinsic breakdown field.

Finally, our trained and validated machine learning model is employed on this downselected set of 209 compounds to make instant predictions of the intrinsic dielectric breakdown strength. The predictions on a set of most promising compounds (i.e., those exhibiting the highest predicted intrinsic dielectric breakdown strength) are further cross-validated via our first-principles framework relying on explicit computation of electron–phonon scattering rates. As a general finding, our analysis reveals that boron containing compounds exhibit remarkable electric field tolerance and are of particular interest. The overall workflow adopted in this study is outlined in Figure 2. In what follows, we describe our findings in greater detail.

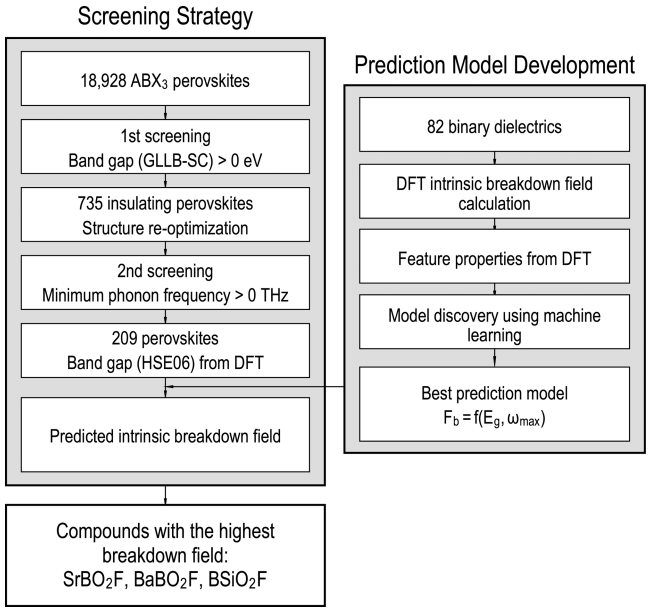

Figure 2. Overall workflow for screening high breakdown field perovskites by the prediction model based on machine learning built on binary dielectrics. The Prediction Model Development procedure is described in ref 26.

THEORETICAL METHODS

In this work, we used first-principles DFT computations to optimize perovskite crystal structures and to compute the band gaps and the phonon frequencies in a high-throughput manner. The DFT calculations were performed using the projector-augmented wave formalism with the local density approximation (LDA)[29] functional as implemented in the Vienna *Ab initio* Simulation Package (VASP).[30] The basis set used included plane waves with kinetic energies up to 450 eV. For

DOI: 10.1021/acs.jpcc.6b05068
J. Phys. Chem. C 2016, 120, 14575−14580

structural optimizations, a Γ-centered Monkhorst−Pack *k*-point mesh of 6 × 6 × 6, giving the Kohn−Sham total energy converged up to 0.5 meV, was used.[31] Relaxations of both the cell shape and internal atomic coordinates were allowed until atomic forces on each of the atoms were smaller than 0.01 eV/Å.

The band gaps of the relaxed structures were computed using the hybrid HSE06 exchange-correlation functional. While spin unpolarized calculations were performed for the close shell systems (identified based on the most commonly exhibited oxidation states of the constituent atoms), spin polarization computations were carried out for the following 14 open-shell compounds, viz. Si_2O_3, $SiGeO_3$, $TiLiO_2N$, $SiNbO_2N$, $InReON_2$, $CsIrN_3$, $GaTaO_2S$, $SiHfO_2S$, $BSiO_2F$, $SiInO_2F$, $AlZrO_2F$, $SiBO_2F$, $GaHfO_2F$, and GaTaONF.

The lattice vibrational spectra at the center of the Brillouin zone, Γ, for these structures were calculated within the density functional perturbation theory (DFPT) formalism as implemented in VASP. The maximum phonon frequencies at the Γ point were then extracted to be used for the prediction of the intrinsic dielectric breakdown. For the band gap and phonon computations, a finer *k*-point mesh of a prespecified spacing parameter h_k = 0.20 Å^{-1} in the reciprocal space was used to adequately handle the Brillouin zones integrations for perovskites with different cell geometries. All DFT results for the ABX_3 compounds considered here are provided in the Supporting Information.

The intrinsic dielectric breakdown field of the most promising perovskites (based on predictions of the machine learning model) was further verified using a recently implemented fully first-principles computational framework. Based on the Fröhlich−von Hippel criterion, the condition for the intrinsic dielectric breakdown field within this framework can be written as

$$A(E, F) > B(E) \quad \text{for all } E \text{ in } \{\text{CBM}, E_i\} \tag{1}$$

where $A(E,F)$ is the rate of the energy gain of an electron of energy E at an electric field F, and $B(E)$ is the rate of energy loss. The threshold energy for impact ionization, E_i, is assumed to be CBM + E_g, where CBM is the conduction band minimum and E_g is the band gap. The intrinsic dielectric breakdown field is the lowest possible field F for which the above condition is satisfied.

The rate of energy gain of the electron can be evaluated as

$$A(E, F) = \frac{e^2\tau(E)F^2}{3m} \tag{2}$$

where e and m are the electronic charge and mass, respectively. $\tau(E)$ is the electron relaxation time due to phonon scattering. Determination of both $\tau(E)$ and $B(E)$ requires a knowledge of the electron−phonon coupling function as explained in previous studies.[22,32]

In the present study, both $\tau(E)$ and $B(E)$ were evaluated at 300 K. All relevant quantities including the intrinsic dielectric breakdown field were computed using DFT within LDA and norm conserving pseudopotentials[33,34] as implemented in the Quantum ESPRESSO code.[35] Electron−phonon coupling function was computed in the linear response regime using density functional perturbation theory (DFPT). A Monkhorst−Pack ***k***-point mesh of 16 × 16 × 16 (to sample the electronic states) and ***q***-point mesh of 4 × 4 × 4 (to sample the phonon states) were used for all materials to obtain converged results.

RESULTS AND DISCUSSION

We start with a data set of 18 928 perovskites reported in the CMR database, each with a prototypical 5-atom ABX_3 unit cell where the motif $X_3 \in \{N_3, O_2F, O_2N, O_2S, O_3, OFN, \text{and } ON_2\}$. Here both A- and B-cation sites are allowed to be occupied by 52 different atomic species. For each of these compounds the CMR database reports band gaps computed using DFT as implemented in the GPAW code[36] with the Gritsenko, van Leeuwen, van Lenthe, and Baerends potential (GLLB),[37] further optimized for solids (-SC) by Kuisma and co-workers.[38] Within this functional, the derivative discontinuity is computed and added back to the Kohn−Sham band gap to correct for the well-known deficiency of conventional local and semilocal DFT that leads to an underestimated band gap. In fact, the GLLB-SC band gaps for several single metal oxides and complex metal oxides have been found in excellent agreement with the corresponding values obtained through direct experimental measurements or using the more advanced and demanding eigenvalue-self-consistent GW approach.[39,40] Since we are primarily interested in insulators, our first screening step simply consists of selecting compounds with a nonzero GLLB-SC band gap. This screening step itself leads to a significant reduction in the total number of compounds with only 735 perovskites (only ∼4% of the entire data set) meeting the downselection criterion.

These 735 insulating cubic perovskites are next subjected to DFT-based structural optimizations, where both cell shape and internal coordinates are allowed to relax. Anticipating that even for a five-atom unit cell a lowered symmetry phase can be more stable, we explicitly relaxed each of these compounds in three different symmetries, namely cubic, tetragonal and rhombohedral crystal symmetries. In addition to choosing an appropriate starting cell geometry for each case, the central B-site cation was given a small (1% of the cubic lattice constant) off-center displacement either along the [001] (for the tetragonal phase) or the along [111] (for the rhombohedral phase) direction. The most favorable cell geometry and the atomic arrangement are then determined by comparing the energetics of the relaxed structures obtained from these three starting geometries.

In our next screening step, we assess dynamical stability of the 735 compounds and further downselect 209 compounds that do not exhibit any soft mode instability at the Γ-point. For computational efficiency of our high throughput exploration, here we operate under the assumption that the zone center modes are representative of the entire Brillouin zone and therefore limit our exploration of phonon frequencies to the Γ-point alone. However, it is important to note that there are known cases where this assumption does not hold true; for example, cubic $SrTiO_3$ is known to have a zero frequency at the Γ-point but imaginary frequencies at at the *M*- and *R*-points existing at the boundary of the Brillouin zone.

A classification summary based on the lattice and point group symmetries of the optimized structures for the 209 dynamically stable insulating perovskite is provided in Table 1. Only 5% of compounds favor the cubic lattice ($Pm\bar{3}m$) as their stable structure, while 27% and 34% of the compounds converged to monoclinic and tetragonal lattices, respectively. The overall workflow described in this section is schematically illustrated in Figure 2. Further details on the machine learning model development can be found in our previous work.[26] The complete data set including structural information, band gap,

DOI: 10.1021/acs.jpcc.6b05068
J. Phys. Chem. C 2016, 120, 14575−14580

Table 1. Classification of Lattice and Point Group Symmetries Obtained by Group Theoretical Analysis for the Dynamically Stable Optimized Perovskite Insulators

lattice	point group	space group (number)	count
triclinic	C_1	$P1$ (1)	20
monoclinic	C_s	Pm (6)	4
	C_s	Cm (8)	51
orthorhombic	C_{2v}	$Pmm2$ (25)	24
	C_{2v}	$Amm2$ (38)	4
tetragonal	C_{4v}	$P4mm$ (99)	63
	D_{4h}	$P4/mmm$ (123)	7
trigonal	C_{3v}	$R3m$ (160)	25
cubic	O_h	$Pm\bar{3}m$ (221)	11

and phonon frequency can be found in the Supporting Information.

In our previous study, the prediction models for the intrinsic dielectric breakdown field were developed using three machine learning methods: kernel ridge regression (KRR),[41−43] random forest regression (RFR),[41] and least absolute shrinkage and selection operator (LASSO)[41,44] methods, using a data set of 82 octet crystalline insulators. After an exhaustive search, the most relevant features controlling the intrinsic dielectric breakdown field were determined to be the band gap and the global maximum of phonon frequencies (phonon cutoff frequency).

Of the three machine learning methods used, the LASSO approach provides an explicit functional form for the intrinsic dielectric breakdown field in terms of the two key descriptors

$$F_b = 24.442 \exp(0.315\sqrt{E_g \omega_{max}}) \quad (3)$$

where F_b is the predicted intrinsic dielectric breakdown field, E_g is the band gap, and ω_{max} is the maximum phonon frequency, specified in units of MV/m, eV, and THz, respectively. In order to apply this prediction model to 209 perovskite dielectrics, we prepared the data set of required features, namely, the band gap and phonon frequency. As the HSE06 band gap is known to predict band gaps with acceptable accuracy, and the maximum phonon frequency typically occurs at the Γ point, these values were used in eq 3. These are reasonable approximations in a first line of screening.

Figure 3 shows the graphical summary of the predicted intrinsic dielectric breakdown field in the property space of HSE06 band gap versus maximum phonon frequency at Γ. The contour for the predicted intrinsic breakdown field, plotted in the Figure 3 using eq 3, may be viewed as a design map that can aid in the rapid screening and identification of dielectrics with high breakdown strength. As presented by eq 3, materials with larger band gap and maximum phonon frequency tend to have larger intrinsic breakdown field. The 209 selected perovskite dielectrics are shown in the figure and distinguished in terms of their crystal structures. Compounds that display the triclinic, monoclinic, and trigonal display the highest breakdown fields.

We further analyzed the correlation between the predicted intrinsic breakdown field and the composition of the 209 perovskites dielectrics. As shown in Figure 4, we show the number of times the 38 elements appear at the two cation (i.e., A and B) sites. For each cation that occurs in the 209 cases, the size of the upper (lower) triangle indicates the number of times it occurs in the A-site (B-site), and the color represents the average breakdown field. From this figure, it is visually obvious that boron, especially when it occurs in the B-site, leads to high

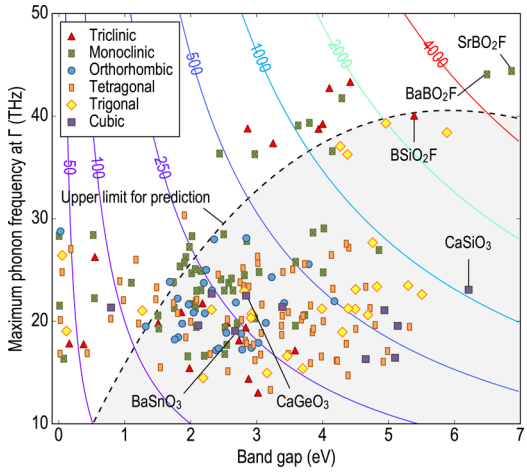

Figure 3. Feature (band gap and maximum phonon frequency at Γ)−property (predicted intrinsic breakdown field) map for 209 perovskites in six crystal structure subclasses. Of the 209 cases, $SrBO_2F$, $BaBO_2F$, and $BSiO_2F$ are identified as promising and worthy of further in-depth studies owing to their high breakdown strength. The shaded region bound by dashed line (given as per eq 3) represents the domain of applicability of the employed interpolative machine learning model within which the dielectric breakdown field is deemed predictable.

breakdown fields. Among all cases, we identify $BaBO_2F$, $SrBO_2F$, and $BSiO_2F$ as candidates worthy of further inquiry.

Before proceeding further, we make the following important observation, concerning the applicability of the LASSO-based breakdown field prediction model to the perovskites class of materials. The shaded region of Figure 3 (bound by a dashed line) shows the E_g−ω_{max} regime within which the dielectric breakdown field is "predictable". This is the regime of the two descriptors (namely, E_g and ω_{max}) occupied by the original 82 binary octet compounds using which the machine learning model of dielectric breakdown field was developed in the first place. It can be seen that several ABX_3 cases fall outside this regime, indicating that the machine learning predictions of the breakdown field for these cases must be viewed with caution.

In particular, the three boron-containing cases, namely, $BaBO_2F$, $SrBO_2F$, and $BSiO_2F$, occur very close to the "predictable" regime boundary. It is thus important to validate the machine learning prediction for these cases, e.g., through direct computation of the breakdown field using DFT. In addition to these cases, we also consider three other cubic perovskites, namely, $CaSiO_3$, $CaGeO_3$, and $BaSnO_3$, which occur well within the predictable regime for additional validation. DFT computations of the breakdown field were performed for all six cases, and these DFT predictions are compared with the machine learning predictions in Figure 5. While the agreement is reasonable for four of the six cases, the two cases, $BaBO_2F$ and $SrBO_2F$, which occur farthest from the predictable regime boundary, lead to the highest discrepancies.

The important finding of this study, nevertheless, is that boron-containing cases may be tolerant to high electric fields, and among those, $BSiO_2F$ and $SrBO_2F$ display breakdown fields of almost 2 GV/m. These compounds may be worthy of further experimental studies.

■ CONCLUSIONS

The intrinsic dielectric breakdown strength of insulators is a key property that dictates performance of electrical and electronic devices. Determination of the breakdown strength

DOI: 10.1021/acs.jpcc.6b05068
J. Phys. Chem. C 2016, 120, 14575−14580

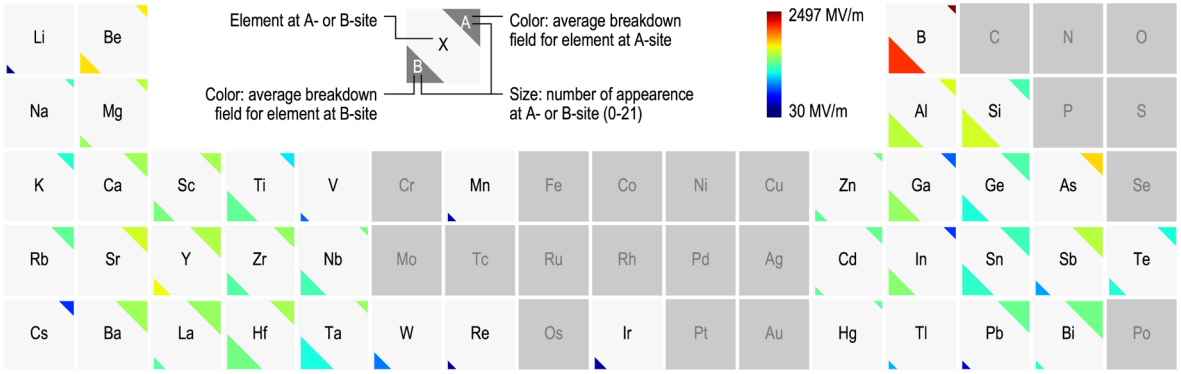

Figure 4. Frequency count for appearance of elements at A- or B-site of 209 dynamically stable insulating perovskites. The largest size of triangle corresponds to the maximum number of appearance, 21, and the smallest size corresponds to the minimum, 1. The elements that are not found from 209 perovskites are shown in gray boxes without triangles. Average of predicted intrinsic breakdown field ranged from 30 to 2497 MV/m is illustrated by the color variation of the triangles.

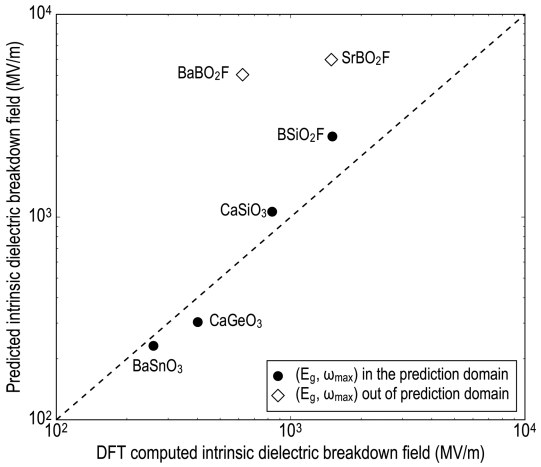

Figure 5. Parity plot comparing the DFT computed intrinsic dielectric breakdown field against the predicted intrinsic breakdown field for three boron-containing cases ($BaBO_2F$, $SrBO_2F$, and $BSiO_2F$) occurring very close to the boundary of the predictable regime and three cubic perovskites ($CaSiO_3$, $CaGeO_3$, and $BaSnO_3$) occurring well within the regime of predictability. The machine learning predicted values for the two perovskites out of predictable regime (i.e., the domain of applicability of the interpolative machine learning model), viz. $SrBO_2F$ and $BSiO_2F$, lead to the highest discrepancies while the other four exhibit a reasonable agreement with the corresponding DFT computed intrinsic dielectric breakdown field.

via a fully first-principles route, although possible, is highly computational-time intensive and therefore impractical for any high throughput screening effort targeted toward identifying promising candidate materials starting from a relatively large set of compounds. Here we have demonstrated that machine learning-based data-enabled approaches can be of particular interest in such situations, providing an efficient alternative pathway for zeroing in on materials of interest. More specifically, in this contribution we screened a large chemical space containing ~19 000 ABX_3, $X_3 \in \{N_3, O_2F, O_2N, O_2S, O_3, OFN, \text{and } ON_2\}$, perovskite compounds. Filtering out metallic and dynamically unstable compounds in a hierarchal down-selection process led to a set of 209 compounds for which the intrinsic breakdown strength was estimated by employing our recently developed machine learning model, which uses the band gap and the maximum phonon cutoff frequency of a given compound to predict its breakdown strength. Further cross-validation of the estimated dielectric breakdown field for the most promising compounds via first-principles DFT computations reveals a reasonable agreement for the compounds that occur well within the predictable regime of the interpolative machine learning model, while discrepancies are found for the compounds occurring out side this domain. An important insight that comes out of this study is that the boron-containing perovskites may be extremely tolerant toward high electric fields; among those, $BSiO_2F$ and $SrBO_2F$ are predicted to display breakdown fields of almost 2 GV/m and therefore worthy of further experimental studies.

■ ASSOCIATED CONTENT

Supporting Information

The Supporting Information is available free of charge on the ACS Publications website at DOI: 10.1021/acs.jpcc.6b05068.

Section S1: data set used for prediction of intrinsic dielectric breakdown field (band gap, phonon frequency, predicted intrinsic dielectric breakdown field, and structural information on 209 dynamically stable insulating perovskites) (PDF)

■ AUTHOR INFORMATION

Corresponding Author

*E-mail: rampi@uconn.edu (R.R.).

Notes

The authors declare no competing financial interest.

■ ACKNOWLEDGMENTS

This paper is based on work supported by the Office of Naval Research through grants N00014-10-1-0944 and N00014-15-1-2665, the former being a Multidisciplinary University Research Initiative (MURI) grant. Computational support was provided by the Extreme Science and Engineering Discovery Environment (XSEDE) and the National Energy Research Scientific Computing Center (NERSC). G.P. acknowledges the support of the U.S. Department of Energy through the LANL/LDRD grant (20140679PRD3) as a Director's postdoctoral fellowship. Ying Sun and Clive Bealing are acknowledged for a prior post-Quantum ESPRESSO code development effort to compute the intrinsic dielectric breakdown field.

DOI: 10.1021/acs.jpcc.6b05068
J. Phys. Chem. C 2016, 120, 14575−14580

REFERENCES

(1) Basic Research Needs for Materials under Extreme Environments. In Report of the Basic Energy Science Workshop on Materials under Extreme Environments: Office of Basic Energy Sciences (Department of Energy), 2007.

(2) Chan, T. Y.; Ko, P. K.; Hu, C. Dependence of Channel Electric Field on Device Scaling. *IEEE Electron Device Lett.* **1985**, *6*, 551−553.

(3) Kittl, J. A.; Opsomer, K.; Popovici, M.; Menou, N.; Kaczer, B.; Wang, X. P.; Adelmann, C.; Pawlak, M. A.; Tomida, K.; Rothschild, A.; et al. High-k Dielectrics for Future Generation Memory Devices. *Microelectron. Eng.* **2009**, *86*, 1789−1795.

(4) Müller, K.; Paloumpa, I.; Henkel, K.; Schmeisser, D. A Polymer High-k Dielectric Insulator for Organic Field-effect Transistors. *J. Appl. Phys.* **2005**, *98*, 056104.

(5) Sharma, V.; Wang, C.; Lorenzini, R. G.; Ma, R.; Zhu, Q.; Sinkovits, D. W.; Pilania, G.; Oganov, A. R.; Kumar, S.; Sotzing, G. A.; Boggs, S. A.; Ramprasad, R. Rational Design of all Organic Polymer Dielectrics. *Nat. Commun.* **2014**, *5*, 4845.

(6) Yang, W. S.; Noh, J. H.; Jeon, N. J.; Kim, Y. C.; Ryu, S.; Seo, J.; Seok, S. I. High-performance Photovoltaic Perovskite Layers Fabricated through Intramolecular Exchange. *Science* **2015**, *348*, 1234−1237.

(7) Ma, R.; Sharma, V.; Baldwin, A. F.; Tefferi, M.; Offenbach, I.; Cakmak, M.; Cao, Y.; Ramprasad, R.; Sotzing, G. A. Rational Design and Synthesis of Polythioureas as Capacitor Dielectrics. *J. Mater. Chem. A* **2015**, *3*, 14845.

(8) Baldwin, A. F.; Huan, T. D.; Ma, R.; Mannodi-Kanakkithodi, A.; Tefferi, M.; Katz, N.; Cao, Y.; Ramprasad, R.; Sotzing, G. A. Rational Design of Organotin Polyesters. *Macromolecules* **2015**, *48*, 2422−2428.

(9) Grinberg, I.; West, D. V.; Torres, M.; Gou, G.; Stein, D. M.; Wu, L.; Chen, G.; Gallo, E. M.; Akbashev, A. R.; Davies, P. K.; Spanier, K. E.; Rappe, A. M. Perovskite Oxides for Visible-light-absorbing Ferroelectric and Photovoltaic Materials. *Nature* **2013**, *503*, 509−512.

(10) Pilania, G.; Wang, C. C.; Wu, K.; Sukumar, N.; Breneman, C.; Sotzing, G.; Ramprasad, R. New Group IV Chemical Motifs for Improved Dielectric Permittivity of Polyethylene. *J. Chem. Inf. Model.* **2013**, *53*, 879−886.

(11) Von Hippel, A. Electric Breakdown of Solid and Liquid Insulators. *J. Appl. Phys.* **1937**, *8*, 815−832.

(12) Fröhlich, H. Theory of Electrical Breakdown in Ionic Crystals. *Proc. R. Soc. London, Ser. A* **1937**, *160*, 230−241.

(13) Seitz, F. On the Theory of Electron Multiplication. *Phys. Rev.* **1949**, *76*, 1376−1393.

(14) Sparks, M.; Mills, D. L.; Warren, R.; Holstein, T.; Maradudin, A. A.; Sham, L. J.; Loh, E.; King, D. F. Theory of Electron-avalanche Breakdown in Solids. *Phys. Rev. B: Condens. Matter Mater. Phys.* **1981**, *24*, 3519−3536.

(15) Osburn, C. M.; Ormond, D. W. Dielectric Breakdown in Silicon Dioxide films on Silicon. *J. Electrochem. Soc.* **1972**, *119*, 591−597.

(16) Honda, K.; Ohsawa, A.; Toyokura, N. Breakdown in Silicon Oxides - Correlation with Cu Precipitates. *Appl. Phys. Lett.* **1984**, *45*, 270.

(17) Grove, A. S.; Leistiko, O.; Sah, C. T. Redistribution of Acceptor and Donor Impurities during Thermal Oxidation of Silicon. *J. Appl. Phys.* **1964**, *35*, 2695−2701.

(18) Deal, B. E.; Grove, A. S.; Snow, E. H.; Sah, C. T. Observation of Impurity Redistribution during Thermal Oxidation of Silicon using the MOS Structure. *J. Electrochem. Soc.* **1965**, *112*, 308.

(19) Ieda, M. Dielectric Breakdown Process of Polymers. *IEEE Trans. Electr. Insul.* **1980**, *EI-15*, 206−224.

(20) Huang, J. S. T.; Welliver, L. C. On the Redistribution of Boron in the Diffused Layer. *J. Electrochem. Soc.* **1970**, *117*, 1577−1580.

(21) Satoh, Y.; Shiota, T.; Murakami, Y.; Shingyouji, T.; Furuya, H. Degradation of Dielectric Breakdown Field of Thermal SiO_2 Films Due to Structural Defects in Czochralski Silicon Substrates. *J. Appl. Phys.* **1996**, *79*, 7944.

(22) Sun, Y.; Boggs, S. A.; Ramprasad, R. The Intrinsic Electrical Breakdown Strength of Insulators from First Principles. *Appl. Phys. Lett.* **2012**, *101*, 132906.

(23) Fröhlich, H. Theory of Dielectric Breakdown. *Nature* **1943**, *151*, 339−340.

(24) Frohlich, H. On the Theory of Dielectric Breakdown in Solids. *Proc. R. Soc. London, Ser. A* **1947**, *188*, 521−532.

(25) Sun, Y.; Bealing, C.; Boggs, S.; Ramprasad, R. 50+ Years of Intrinsic Breakdown. *IEEE Elect. Insul. Mag.* **2013**, *29*, 8−15.

(26) Kim, C.; Pilania, G.; Ramprasad, R. From Organized High-throughput Data to Phenomenological Theory using Machine Learning: The Example of Dielectric Breakdown. *Chem. Mater.* **2016**, *28*, 1304−1311.

(27) Landis, D. D.; Hummelshøj, J. S.; Nestorov, S.; Greeley, J.; Dułak, M.; Bligaard, T.; Nørskov, J. K.; Jacobsen, K. W. The Computational Materials Repository. *Comput. Sci. Eng.* **2012**, *14*, 51−57.

(28) Heyd, J.; Scuseria, G. E.; Ernzerhof, M. Hybrid Functionals based on a Screened Coulomb Potential. *J. Chem. Phys.* **2003**, *118*, 8207−8215.

(29) Blöchl, P. E. Projector Augmented-wave Method. *Phys. Rev. B: Condens. Matter Mater. Phys.* **1994**, *50*, 17953−17979.

(30) Kresse, G.; Hafner, J. Ab Initio Molecular Dynamics for Liquid Metals. *Phys. Rev. B: Condens. Matter Mater. Phys.* **1993**, *47*, 558−561.

(31) Monkhorst, H.; Pack, J. Special Points for Brillouin Zone Integrations. *Phys. Rev. B* **1976**, *13*, 5188−5192.

(32) Sjakste, J.; Vast, N.; Tyuterev, V. Ab Initio Method for Calculating Electron-phonon Scattering Times in Semiconductors: Application to GaAs and GaP. *Phys. Rev. Lett.* **2007**, *99*, 236405.

(33) Perdew, J. P.; Wang, Y. Accurate and Simple Analytic Representation of the Electron-gas Correlation Energy. *Phys. Rev. B: Condens. Matter Mater. Phys.* **1992**, *45*, 13244−13249.

(34) Ceperley, D. M.; Alder, B. J. Ground State of the Electron Gas by a Stochastic Method. *Phys. Rev. Lett.* **1980**, *45*, 566−569.

(35) Giannozzi, P.; Baroni, S.; Bonini, N.; Calandra, M.; Car, R.; Cavazzoni, C.; Ceresoli, D.; Chiarotti, G. L.; Cococcioni, M.; Dabo, I.; et al. Quantum Espresso: A Modular and Open-source Software Project for Quantum Simulations of Materials. *J. Phys.: Condens. Matter* **2009**, *21*, 395502.

(36) Mortensen, J. J.; Hansen, L. B.; Jacobsen, K. W. Real-space Grid Implementation of the Projector Augmented Wave Method. *Phys. Rev. B: Condens. Matter Mater. Phys.* **2005**, *71*, 035109.

(37) Gritsenko, O.; Van Leeuwen, R.; Van Lenthe, E.; Baerends, E. J. Self-consistent Approximation to the Kohn-Sham Exchange Potential. *Phys. Rev. A: At., Mol., Opt. Phys.* **1995**, *51*, 1944−1954.

(38) Kuisma, M.; Ojanen, J.; Enkovaara, J.; Rantala, T. T. Kohn-Sham Potential with Discontinuity for Band Gap Materials. *Phys. Rev. B: Condens. Matter Mater. Phys.* **2010**, *82*, 115106.

(39) Castelli, I. E.; Olsen, T.; Datta, S.; Landis, D. D.; Dahl, S.; Thygesen, K. S.; Jacobsen, K. W. Computational Screening of Perovskite Metal Oxides for Optimal Solar Light Capture. *Energy Environ. Sci.* **2012**, *5*, 5814.

(40) Castelli, I. E.; Hüser, F.; Pandey, M.; Li, H.; Thygesen, K. S.; Seger, B.; Jain, A.; Persson, K. A.; Ceder, G.; Jacobsen, K. W. New Light-harvesting Materials using Accurate and Efficient Bandgap Calculations. *Adv. Energy Mater.* **2015**, *5*, 1400915.

(41) Hastie, T.; Tibshirani, R.; Friedman, J. *The Elements of Statistical Learning: Data Mining, Inference, and Prediction*, 2nd ed.; Springer: New York, 2009.

(42) Muller, K.-R.; Mika, S.; Ratsch, G.; Tsuda, K.; Scholkopf, B. An Introduction to Kernel-based Learning Algorithms. *IEEE Trans. Neural Netw.* **2001**, *12*, 181−201.

(43) Hofmann, T.; Schölkopf, B.; Smola, A. J. Kernel Methods in Machine Learning. *Ann. Stat.* **2008**, *36*, 1171−1220.

(44) Tibshirani, R. Regression Selection and Shrinkage via the LASSO. *J. R. Stat. Soc., Ser. B* **1994**, *58*, 267−288.

DOI: 10.1021/acs.jpcc.6b05068
J. Phys. Chem. C 2016, 120, 14575−14580